Numerical Simulation of Breaking Waves Using Adaptive Mesh Approach

Cheng Liu[1,*], Changhong Hu[2,*]

[*]*Research Institute for Applied Mechanics, Kyushu University, Fukuoka 816-0811, Japan*
[1]*Email:liu@riam.kyushu-u.ac.jp,* [2]*Email:hu@riam.kyushu-u.ac.jp*

1. Introduction

Strongly nonlinear interaction between wave and floating body is an important problem in many ocean and offshore engineering applications. However, numerical simulation of such problem is still very challenging, since the wave turbulence, wave breaking, air entrainment, droplet and bubbles should be considered together [1].

The CFD solver we are developing is for distributed memory parallel computer system. High parallelization efficiency of the blocked adaptive mesh (BAMR) solver is the point of our concern. Main features of the solver are summarized as follows. First, we extend VOF/PLIC [2] and THINC [3] scheme to adapt to the adaptive mesh frameworks for sharp representation of moving distorted interfaces. Second, to preserve the flux conservation, a conservative prolongation approach is proposed for filling the fluxes in newly created cells. Third, we improve the accuracy of calculating curvature from volume fraction field by using height function method [4]. Forth, a fast algorithm for generating the coefficient matrix of elliptic operator, which is based on adaptive mesh topology, is proposed. Different from other methods, our algorithm is specially designed for blocked mannered adaptive meshes, in which the matrix assembling occupies a very small portion of the total running time. In this paper, some of the recently obtained results by the BAMR solver are presented.

Our BAMR framework has been adopted for solving compressible Euler equation [5], compressible multi-medium flows [6] and incompressible flows with IB (immersed boundary) method. Now we are extending the AMR framework for free surface flows with consideration of the surface tension effect.

2. Mathematical Formulation

In present study the interface is represented by volume fraction field $\mathcal{F}(0 \le \mathcal{F} \le 1)$. The piecewise linear interface calculation (PLIC) method is applied for reconstruction of the interface inside a cell. $\mathcal{F}$ is evolved by

$$\frac{\partial \mathcal{F}}{\partial t} + \nabla \cdot (\mathbf{u}\mathcal{F}) = 0. \tag{1}$$

Considering the following integral form of the incompressible Navier-Stokes equation,

$$\int_\Gamma \mathbf{u} \cdot \mathbf{n}\, dS = 0, \tag{2}$$

$$\frac{\partial}{\partial t}\int_\Omega \mathbf{u}\, dV + \int_\Gamma \mathbf{u}\,(\mathbf{u}\cdot\mathbf{n}) dS = \frac{1}{\rho}\int_\Gamma p\mathbf{n}\, dS + \frac{1}{\rho}\int_\Gamma \boldsymbol{\tau}\cdot\mathbf{n}\, dS + \frac{1}{\rho}\mathbf{F}_s + \frac{1}{\rho}\mathbf{F}_g, \tag{3}$$

where $\mathbf{n}$ is the unit normal vector, Γ the control surface, Ω the control volume enclosed by Γ. $\mathbf{u}$ and p indicate the velocity vector and pressure, respectively. $\boldsymbol{\tau} = \mu[\nabla\mathbf{u} + (\nabla\mathbf{u})^T]$ is the shear stress tensor. $\mu(\mathcal{F})$ represents the viscosity and $\rho(\mathcal{F})$ is the density of the fluid. $\mathbf{F}_s$ and $\mathbf{F}_g$ is body force,

while $\mathbf{F}_s$ is the surface tension force which can be written as

$$\mathbf{F}_s = \sigma \mathcal{K} \mathbf{n} \tag{4}$$

where σ is the surface tension coefficient and $\mathcal{K}$ is the local curvature of the interface. $\mathcal{K}$ is obtained from height function method [4].

A fractional step method with second order accuracy is adopted for decoupling pressure and velocity. Solution of Eqs. (2-3) is split into three steps.

a. Prediction of intermediate velocity $\mathbf{u}''$.

a-1: Advection part,

$$\frac{\partial}{\partial t}\int_{\Omega} \mathbf{u}' \, dV + \int_{\Gamma} \mathbf{u}^{n-1} (\mathbf{u}^{n-1} \cdot \mathbf{n}) dS = 0, \tag{5}$$

a-2: Non-advection part,

$$\frac{\partial}{\partial t}\int_{\Omega} \mathbf{u}'' \, dV - \frac{1}{\rho}\int_{\Gamma} \boldsymbol{\tau} \cdot \mathbf{n} \, dS = \frac{1}{\rho}\mathbf{F}_s + \frac{1}{\rho}\mathbf{F}_g, \tag{6}$$

b. Imposing incompressibility constraint.

$$\frac{1}{\rho}\int_{\Omega} \nabla p^n \cdot \mathbf{n} \, dS = \frac{1}{\Delta t}\int_{\Gamma} \mathbf{u}'' \cdot \mathbf{n} dS, \tag{7}$$

c. Correction to get final velocity field $\mathbf{u}^n$ that satisfy the divergence free conditions.

$$\frac{\partial}{\partial t}\int_{\Omega} \Delta \mathbf{u}^n \, dV = \frac{1}{\rho}\int_{\Gamma} p^n \mathbf{n} dS, \tag{8}$$

where $\Delta \mathbf{u}^n$ is the compensation from pressure gradient. The multi-moment FVM [7] is adopted for spatial discretization of Eqs. (5-8).

3. Numerical Method

Unlike conventional FVM, which utilizes cell-integrated value only, the multi-moment FVM builds high order spatial approximation by introducing 'moments' [7] in a cell, which makes the solver less diffusive, more robust and more compact. In this study the formulation of CIP-CSL2 [7] is used for discretization of the advection part.

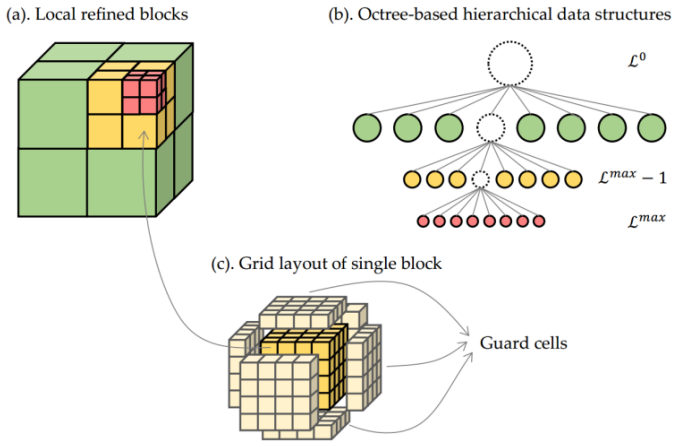

Fig. 1 3-D adaptive mesh and its representation as an octree.

In block-structured adaptive mesh, the basic unit for manipulation is the blocks as shown in Fig. 2 (a) (c). The computational domain is discretized on a series of block $\mathcal{B}_{\mathcal{L}}, (\mathcal{L} = 0,1, \ldots, \mathcal{L}^{max})$, where $\mathcal{B}_0$

is the coarsest level and the level $\mathcal{L}+1$ is finer than the level $\mathcal{L}$ with the factor of 2.To manage the block topology efficiently, the octree-based hierarchical data structure is used (Fig. 2 (b)). Numerical solution is advanced only on $\{\mathcal{B}_{\mathcal{L}} \mid \forall \mathcal{B}_{\mathcal{L}} \in \Omega_L\}$, which is indicated by the solid circles in Fig. 2 (b). Different from the overlapped grid topology, physical memory required by the current method is allocated only in $\{\mathcal{B}_{\mathcal{L}} \mid \forall \mathcal{B}_{\mathcal{L}} \in \Omega_L\}$, and no memory space is allocated for the nodes marked with dotted circle in Fig. 2 (b). The Peano and Hilbert space-filling curves are generated based on the octree for achieving a dynamically loading balance among the processors [8].

4. Numerical Results

The two-phase flow solver is validated by two benchmark tests. We use the case of a small-amplitude capillary wave problem (no gravity) to estimate the accuracy of present surface tension model. Then a free surface oscillation test is performed to validate the accuracy in prediction of pure gravity driven flows. It can be expected that due to the viscous effect, the wave oscillation will be attenuated. The computational domain is $x \in [-0.5\lambda, 0.5\lambda]$, $y \in [-1.5\lambda, 1.5\lambda]$, here λ is the wavelength of the perturbation. The initial wave profile is defined as $H(x,t_0) = A_0\cos(kx)$, here the perturbation amplitude $A_0 = \lambda/100$, the wave number $k = 2\pi/\lambda$. The relative maximum interface height varying with time is presented in Fig. 2. Theoretical solution of the wave amplitude is derived from the theoretical analysis [9], which is indicated by the solid red line. The hollow circles are obtained from present BAMR solver.

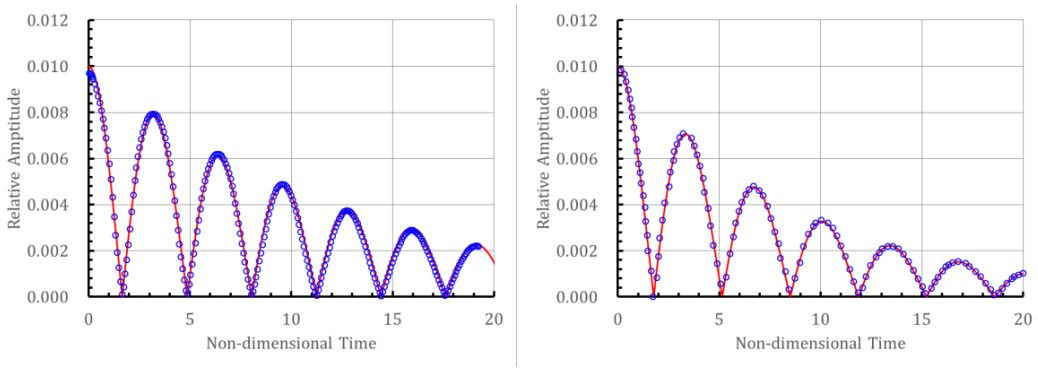

Fig. 2 Evolution of the amplitude of the wave profile as a function of non-dimensional time τ, (a) capillary wave, $La = 3000$, $\rho_l/\rho_g = 1000.0/1.2$, $\mu_l/\mu_g = 1.0\times10^{-3}/1.8\times10^{-5}$, $g = 0$ (b) gravity wave, $\rho_l/\rho_g = 10$, $\rho_l/\rho_g = 1.0$, $g = 50$. –: A. Prosperetti's theoretical solution [9], ○: results of present BAMR solver.

Finally, a wave breaking problem is investigated numerically by present BAMR solver. To save the computational load, the periodic boundary condition is specified on the left and right boundary of the numerical tank, as seen in Fig. 3. The computational domain is $x, z \in [-0.5\lambda, 0.5\lambda]$, $y \in [-0.125\lambda, 0.125\lambda]$, where λ is the wavelength of the initial free surface. During the simulation, the cells corresponding with the free surface are always covered by finest blocks, as shown in Fig. 3 (e), each block is filled with $8\times8\times8$ uniform Cartesian grids. The free surface profiles evolved with time are given in Fig. 3 (a-d).

5. Summary

In this manuscript, we present our new developments on an adaptive mesh refinement solver for incompressible free surface flows. Several preliminary validation tests show that the present numerical

approach is efficient for simulation of incompressible free surface flows. This is an ongoing development, more newly obtained numerical results will be presented at the workshop.

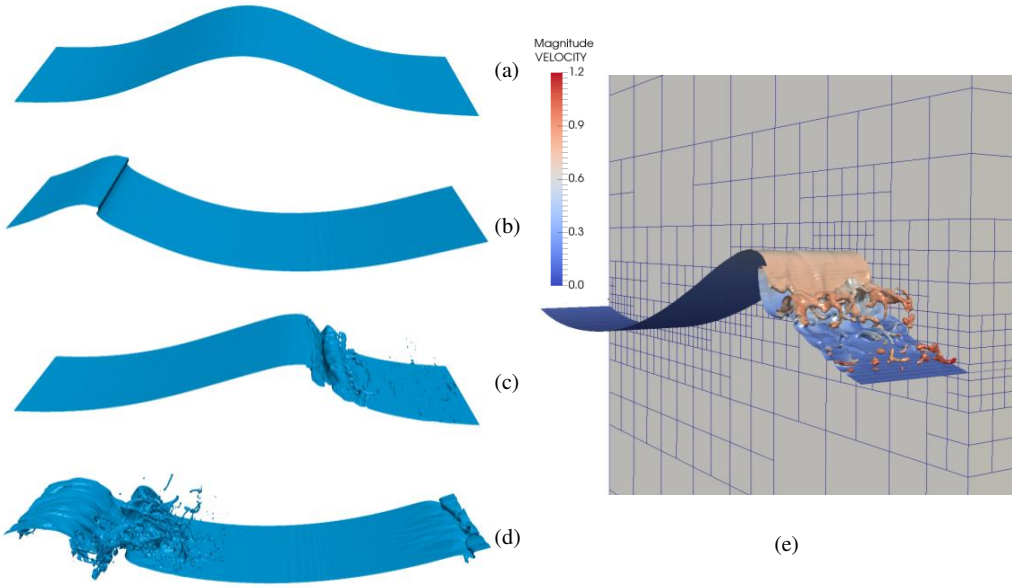

Fig. 3 Wave profiles at different time. (a) $t = 0$, (b) $t = 0.24$, (c) $t = 0.40$, (d) $t = 0.52$, (e) blocks for AMR and free surface colored by velocity distribution.

Acknowledgements

Reference

[1]. Scardovelli R, Zaleski S. Direct numerical simulation of free-surface and interfacial flow. *Annual Review of Fluid Mechanics*, 1999, 31(1): 567-603.

[2]. Gueyffier D, Li J, Nadim A, et al. Volume-of-fluid interface tracking with smoothed surface stress methods for three-dimensional flows. *Journal of Computational physics*, 1999, 152(2): 423-456.

[3]. Xiao F, Ii S, Chen C. Revisit to the THINC scheme: a simple algebraic VOF algorithm. *Journal of Computational Physics*, 2011, 230(19): 7086-7092.

[4]. Popinet S. An accurate adaptive solver for surface-tension-driven interfacial flows. *Journal of Computational Physics*, 2009, 228(16): 5838-5866.

[5]. Liu C, Hu C. An Immersed Boundary Solver for Inviscid Compressible Flows. *International Journal for Numerical Methods in Fluids*. Doi: 10.1002/fld.4399.

[6]. Liu C, Hu C. Adaptive THINC-GFM for compressible multi-medium flows. *Journal of Computational Physics*, 2017, 342: 43-65.

[7]. Xiao F, Ikebata A, Hasegawa T. Numerical simulations of free-interface fluids by a multi-integrated moment method. *Computers & structures*, 2005, 83(6): 409-423.

[8]. MacNeice P, Olson K M, Mobarry C, et al. PARAMESH: A parallel adaptive mesh refinement community toolkit. *Computer Physics Communications*, 2000, 126(3): 330-354.

[9]. Prosperetti A. Motion of two superposed viscous fluids. *Physics of Fluids*, 1981, 24(7): 1217-1223.